RESEARCH ARTICLE

A Pervasive Millennial-Scale Cycle in North Atlantic Holocene and Glacial Climates

Gerard Bond,* William Showers, Maziet Cheseby, Rusty Lotti, Peter Almasi, Peter deMenocal, Paul Priore, Heidi Cullen, Irka Hajdas, Georges Bonani

Evidence from North Atlantic deep sea cores reveals that abrupt shifts punctuated what is conventionally thought to have been a relatively stable Holocene climate. During each of these episodes, cool, ice-bearing waters from north of Iceland were advected as far south as the latitude of Britain. At about the same times, the atmospheric circulation above Greenland changed abruptly. Pacings of the Holocene events and of abrupt climate shifts during the last glaciation are statistically the same; together, they make up a series of climate shifts with a cyclicity close to 1470 ± 500 years. The Holocene events, therefore, appear to be the most recent manifestation of a pervasive millennial-scale climate cycle operating independently of the glacial-interglacial climate state. Amplification of the cycle during the last glaciation may have been linked to the North Atlantic's thermohaline circulation.

More than 20 years ago, Denton and Karlén (*1*) made two provocative suggestions about the climate of our present interglacial or Holocene period. Having found what appeared to be synchronous advances of mountain glaciers in North America and Europe, they concluded that Holocene climate was much more variable than implied by broad trends in pollen and marine records. On the basis of radiocarbon chronologies of the glacial advances, they further suggested that the climate variations were part of a regular millennial-scale pattern, which when projected backward coincided with climate shifts of the preceding glaciation and when projected forward predicted a progressive warming over the next few centuries.

Despite its important implications, Denton and Karlén's concept of a predictable, millennial-scale climate rhythm has not been widely accepted, partly because it has been difficult to find corroborating evidence in other climate records. For example, measurements of oxygen isotopes, methane concentrations, and snow accumulation in Greenland ice cores reveal no evidence of millennial-scale fluctuations during the Holocene, except perhaps for a brief cooling about 8200 years ago (*2*). Many researchers now view the Holocene climate as anomalously stable (*3*). Recent evidence from deep sea sediments in the Nordic Seas (*4*) suggests that Holocene climate there was even more stable than climate during the last interglaciation (Eemian).

In 1995, however, O'Brien *et al.* (*5*) demonstrated from measurements of soluble impurities in Greenland ice that Holocene atmospheric circulation above the ice cap was punctuated by a series of millennial-scale shifts. The most prominent of those shifts appeared to correlate with Denton and Karlén's glacial advances. Encouraged by the findings of O'Brien and her colleagues, we launched an investigation of deep sea Holocene sediments in the North Atlantic, anticipating that the shifts in atmospheric circulation above the ice cap were part of a much larger climate pattern that left its imprint in the deep sea record. Here, we report the results of that investigation, showing that the North Atlantic's Holocene climate indeed exhibits variability on millennial scales, and we then compare the Holocene variations with climate shifts of the last glaciation.

We analyzed Holocene sediment in two cores from opposite sides of the North Atlantic (Fig. 1), VM 28-14 (64°47′N, 29°34′W; 1855 m of depth) and VM 29-191 (54°16′N, 16°47′W; 2370 m of depth). High-resolution accelerator mass spectrometer radiocarbon datings of planktonic foraminifera demonstrate that both cores have thick and nearly complete Holocene sections (Table 1 and Fig. 2). Core top ages are less than 1000 years (all ages are in calendar years B.P. unless otherwise indicated). Sedimentation rates in both cores exceeded 10 cm per 1000 years, more than sufficient to resolve millennial-scale variability, and the rates were nearly constant (Fig. 2). We sampled both cores at intervals of 0.5 to 1 cm (equivalent to a resolution of 50 to 100 years), and in each sample we measured nine proxies (*6*).

The Holocene signal: Episodes of ice-rafting. The most conspicuous evidence of variations in the North Atlantic's Holocene climate comes from the same three proxies that we used to document ice-rafting in the North Atlantic during the last glaciation (*7*). One proxy is the concentration of lithic grains, defined as the number of grains with diameters greater than 150 μm in 1 g of core. At both sites we found a series of increases in grain concentrations, which, although of much smaller magnitude than those of the last glaciation, are distinct and reach peak values several times that of the ambient grain concentrations (Fig. 2).

The other two proxies are petrologic tracers, defined as the percentages of certain types of lithic grains. One of the tracers is fresh volcanic glass, which comes from Iceland or Jan Mayen, and the other is hematite-stained grains, mostly quartz and feldspar, that come from sedimentary deposits containing red beds (Fig. 3) (*7*). During each of the lithic events, both tracers display prominent increases well above the 2σ counting error (Fig. 2) (*8*).

These lithic/petrologic events demonstrate that ice-rafting episodes also occurred during the Holocene. Age differences of lithic/petrologic maxima between the two sites are within the 2σ calendar age error (Fig. 2 and Table 1); hence, the events cannot be local in origin. Regional changes in carbonate dissolution or in winnowing of fine sediment could not have produced the petrologic changes we measured, and in neither core could we find evidence of current laminations or cross-bedding, making it unlikely that the events were produced by strong bottom currents [see also caveats in (*9*)].

Hence, contrary to the conventional view, the North Atlantic's Holocene climate must have undergone a series of abrupt reorganizations, each with sufficient impact to force concurrent increases in debris-bearing drift ice at sites more than 1000 km apart and overlain today by warm, largely ice-free surface waters of the North Atlantic and Irminger currents. The ice-rafted debris (IRD) events exhibit a distinct pacing on millennial scales, with peaks at about 1400, 2800, 4200, 5900, 8100, 9400,

G. Bond, M. Cheseby, R. Lotti, P. Almasi, P. deMenocal, P. Priore, and H. Cullen are at the Lamont-Doherty Earth Observatory of Columbia University, Route 9W, Palisades, NY 10964, USA. W. Showers is in the Department of Marine, Earth and Atmospheric Sciences, North Carolina State University, 1125 Jordan Hall, Raleigh, NC 27695, USA. I. Hajdas and G. Bonani are in the AMS ^{14}C Lab, ITP Eidgenössische Technische Hochschule (ETH) Honeggerberg, CH-8093 Zurich, Switzerland.

*To whom correspondence should be addressed. E-mail: gcb@lamont.ldgo.columbia.edu

10,300, and 11,100 years ago.

Ocean forcing of the Holocene signal. We argue that the immediate cause of the Holocene ice-rafting events was a series of ocean surface coolings, each of which appears to have been brought about by a rather substantial change in the North Atlantic's surface circulation. The most consistent evidence of ocean surface coolings is the succession of prominent increases in *Globigerina quinqueloba* (Fig. 2), a species that today dominates the planktonic foraminiferal populations in cool Arctic waters north of Iceland (*10*). Corroborating that evidence are increases in abundances of *Neogloboquadrina pachyderma* (s.), the polar planktonic foraminifera, during the first four events (events 5 to 8), and marked decreases in abundances of the warm-water planktonic species *N. pachyderma* (d.) during middle and late Holocene events (Fig. 2). Although some of the faunal shifts are not large, all are defined by more than one species, and they are correlative at two widely separated sites. Moreover, because the foraminiferal concentrations increased markedly during most events (Fig. 2), it is unlikely that the assemblages were modified by carbonate dissolution.

Analysis of stable isotopes in *G. bulloides* and *N. pachyderma* (d.) in the two cores produced isotopic evidence of cooling at the level of the Younger Dryas event—as

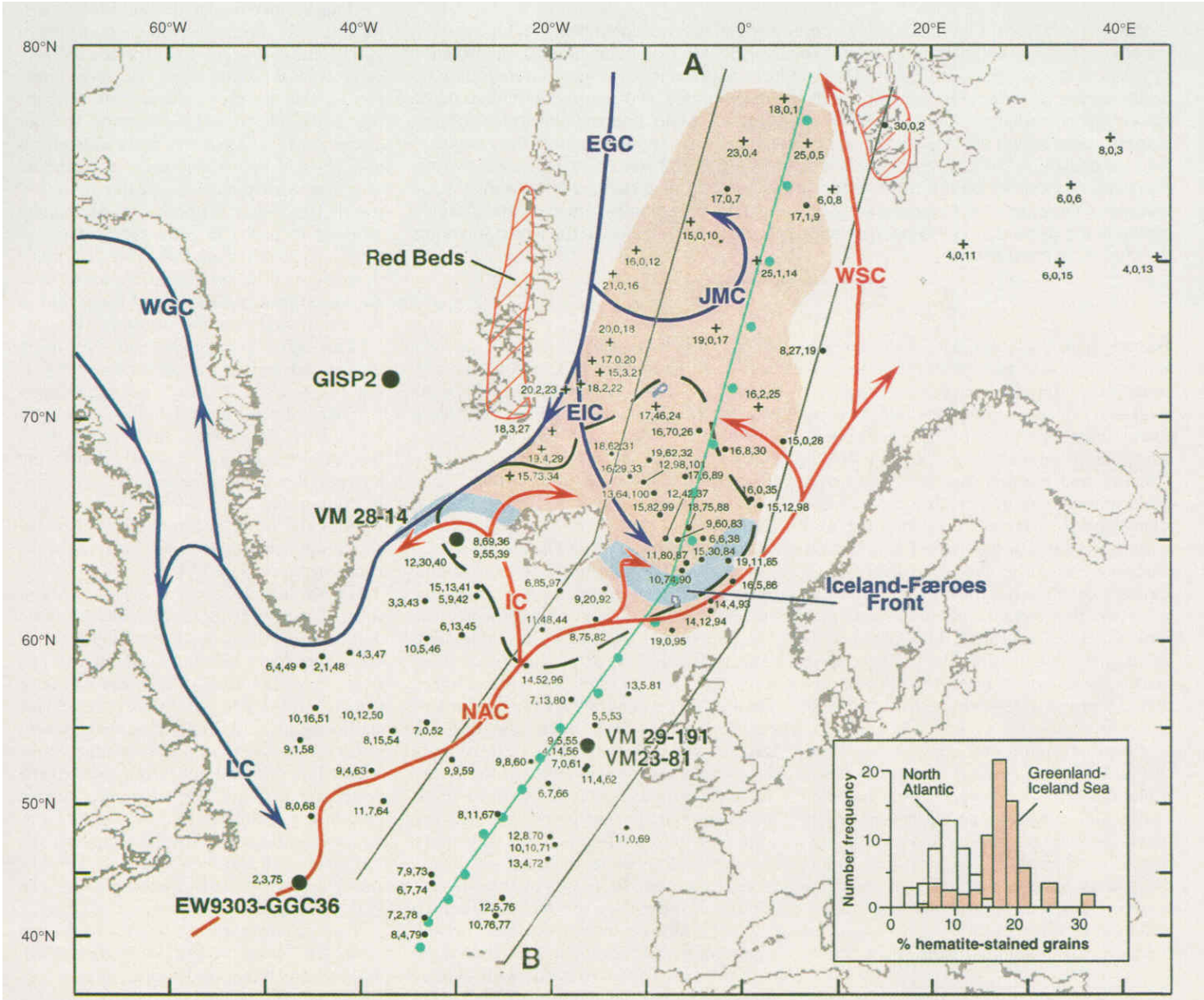

Fig. 1. Location of cores we analyzed and principal surface currents in the North Atlantic and Nordic Seas. The green dots and green line are locations of COADS temperature estimates and the profile in Fig. 4A. The line from A to B is the line of the cross section of petrologic data shown in Fig. 4B. Small dots and plus signs are locations of core tops analyzed for the two petrologic tracers; numbers (from left to right) are percentage of hematite-stained grains, percentage of Icelandic glass, and core locator number [core locations and site numbers can be obtained from the first author; see also (*17*)]. Shaded red area encloses core tops with ≥10% hematite-stained grains. Dashed black line encloses core tops with ≥15% Icelandic glass. Histogram insert summarizes core top data for hematite-stained grains showing contrast in percentages north and south of the Denmark Strait and Iceland-Faeroes frontal systems, indicated by blue shading. Locations of red beds in East Greenland and Svalbard are from (*7*). Surface currents: EGC, East Greenland Current; JMC, Jan Mayen Current; WSC, West Spitsbergen Current; EIC, East Iceland Current; WGC, West Greenland Current; LC, Labrador Current; NAC, North Atlantic Current; IC, Irminger Current.

1258 SCIENCE • VOL. 278 • 14 NOVEMBER 1997 • www.sciencemag.org

much as 5°C if the isotopic enrichment was entirely the result of a temperature change (*11*)—but revealed little variability during any of the Holocene events at either coring site (Fig. 2). The cooler surface waters may have been fresher, thereby offsetting temperature-driven $\delta^{18}O$ enrichment, or cooler surface waters may have forced planktonic species to shift growth seasons or depth habitats, as recently documented for *N. pachyderma* (s.) in the North Atlantic (*12*). Whatever the reason, at least in the subpolar North Atlantic, planktonic isotopic compositions apparently are not robust indicators of variability during present-day interglacial climates.

The magnitudes of the ocean surface coolings probably did not exceed 2°C, at least in the eastern North Atlantic; this conclusion is based on a comparison of planktonic abundances in VM 29-191 and recent measurements of modern (core top) assemblages in the Nordic Seas (Fig. 4A). We chose not to further quantify ocean surface temperatures with transfer function methods because their errors are relatively large (*13*), and in an earlier effort at VM 28-14, results were uncertain because of no-analog problems (*14*). If this upper limit is correct, the Holocene coolings did not exceed 15 to 20% of the full Holocene-to-glacial temperature change (*15*).

The strongest evidence for changes in ocean surface circulation during the ice-rafting events comes from VM 29-191. Today, most of the ice entering the subpolar North Atlantic is calved in southern and western Greenland, circulates through the southwestern part of the subpolar gyre in the Labrador Sea, and enters the North Atlantic near Newfoundland (Fig. 1) (*16*). If present-day circulation remained unchanged during the Holocene, IRD at VM 29-191 and in Labrador Sea ice should have similar compositions. However, in the broad area south of Iceland where Labrador Sea ice is dispersed (*16*), percentages of the two tracers in modern (core top) IRD are consistently lower than even their mean values in VM 29-191 [Fig. 1; see also (*17*)]. In core GGC36, which contains debris from icebergs exiting the Labrador Sea, percentages of the two tracers exhibit similar low values throughout almost the entire Holocene (Figs. 1 and 5).

We find instead that the sources of IRD at VM 29-191 must have been much farther to the northeast in the Greenland-Iceland seas. There, percentages of the two tracers in core top sediments consistently reach or even exceed their peak values in VM 29-191 (Figs. 1 and 4B). The Icelandic material probably was erupted onto drifting ice [see also (*18*)], and hematite-stained grains may have come from along coastal East

Table 1. Accelerator mass spectrometer radiocarbon measurements and calibrated (calendar) ages.

Depth (cm)	Species	Corrected radiocarbon age*	Calendar age†	2σ age range
		VM 29-191		
*f*1	*G. bulloides*	990 ± 55	868	752–983
*f*21	*G. bulloides*	2,825 ± 60	2,928	2,779–3,077
*f*41	*G. bulloides*	5,355 ± 75	6,136	5,984–6,288
*f*61	*G. bulloides*	7,600 ± 80	8,334	8,168–8,499
*f*81.2	*G. bulloides*	8,895 ± 80	9,714	9,651–9,776
*f*91	*G. bulloides*	9,175 ± 95	10,166	9,979–10,353
≠111	Mixed planktonic	10,150 ± 55	10,931	10,854–11,007
≠121	*N. pachyderma* (s.)	10,950 ± 50	12,459	12,281–12,637
≠125	Mixed planktonic	11,450 ± 45	12,962	12,829–13,094
		VM 28-14		
¡8	*G. bulloides*	1,643 ± 60	1,516	1,396–1,635
*f*19.5	*G. bulloides*	2,895 ± 60	3,019	2,862–3,175
¡32	*G. bulloides*	3,540 ± 53	3,809	3,687–3,931
¡44	*G. bulloides*	4,318 ± 59	4,931	4,816–5,046
*f*52	*G. bulloides*	4,895 ± 70	5,659	5,561–5,757
¡60	*G. bulloides*	5,515 ± 51	6,337	6,264–6,410
*f*74	*G. bulloides*	6,680 ± 80	7,507	7,390–7,623
*f*76.7	*G. bulloides*	7,100 ± 75	7,854	7,707–8,001
*f*82	*G. bulloides*	8,010 ± 80	8,788	8,558–9,017
‡90	*N. pachyderma* (s.)	8,810 ± 140	9,749	9,494–10,004
‡95	*N. pachyderma* (s.)	10,290 ± 130	11,906	11,329–12,483
‡103	*N. pachyderma* (s.)	10,880 ± 130	12,797	12,521–13,072
‡108	*N. pachyderma* (s.)	11,040 ± 130	12,960	12,684–13,235
		VM 23-81		
‡157	*N. pachyderma* (s.)	10,880 ± 90	12,651	12,597–12,704
‡160	*N. pachyderma* (s.)	10,980 ± 150	12,900	12,586–13,213
‡172	*N. pachyderma* (s.)	11,580 ± 110	13,531	13,240–13,822
*f*205	*N. pachyderma* (s.)	12,180 ± 100	14,243	13,882–14,603
*f*210	*N. pachyderma* (s.)	13,440 ± 120	16,068	15,689–16,447
*f*219	*N. pachyderma* (s.)	13,630 ± 100	16,325	16,009–16,641
*f*221	*N. pachyderma* (s.)	14,150 ± 110	16,965	16,658–17,272
*f*223	*N. pachyderma* (s.)	14,330 ± 100	17,176	16,894–17,457
*f*227	*N. pachyderma* (s.)	14,770 ± 110	17,669	17,378–17,960
*f*229	*N. pachyderma* (s.)	15,040 ± 110	17,744	17,674–17,814
*f*251	*N. pachyderma* (s.)	15,650 ± 150	18,552	18,222–18,881
*f*263	*N. pachyderma* (s.)	17,280 ± 130	20,511	20,003–21,018
*f*274	*N. pachyderma* (s.)	17,875 ± 150	21,305	20,774–21,835
¡287.5	*N. pachyderma* (s.)	18,269 ± 163	21,820	21,299–22,340
¡H2-328		20,780 –	24,000	–
¡H3-381		26,270 –	30,000	–
		VM 19-30		
*f*100	Mixed planktonic	12,430 ± 90	14,571	14,201–14,940
*f*150	Mixed planktonic	17,500 ± 130	20,808	20,307–21,308
*f*198.5	Mixed planktonic	22,730 ± 190	26,562	–
*f*249.5	*N. pachyderma* (d.)	28,090 ± 250	30,249	–
*f*297.4	Mixed planktonic	31,310 ± 390	34,847	–
*f*350	Mixed planktonic	37,640 ± 610	42,845	–
		GGC36		
*f*1	*G. bulloides*	2,540 ± 70	2,087	2,220–1,954
¡15	*G. bulloides*	5,422 ± 75	5,850	5,997–5,703
*f*30	*G. inflata*	7,720 ± 100	8,070	8,218–7,922
¡50	*G. bulloides*	8,146 ± 90	8,526	8,725–8,327
*f*60	*G. inflata*	8,720 ± 100	9,268	9,453–9,082
¡87.5	*G. inflata*	9,052 ± 88	9,662	9,871–9,452
*f*90	*G. inflata*	8,580 ± 95	9,166	9,387–8,945
*f*120	*G. inflata*	9,165 ± 85	9,725	9,924–9,525
¡140	*G. inflata*	10,555 ± 138	11,665	12,264–11,065
*f*150	*G. inflata*	10,750 ± 95	12,110	12,526–11,694

*Corrected by −400 years for the age of the surface ocean reservoir, except for VM 19-30 for which the correction is −500 years. †Radiocarbon ages to 18,800 years calibrated according to (*46*). *f* from ETH, Zurich; ≠ from (*61*); ‡ from (*62*); ¡, from Arizona; !, interpolated radiocarbon ages from (*7*) and calibrated according to (*24*). Of the three Barbados corals dated beyond 18,000 radiocarbon years, one has a radiocarbon age of 26,160 ± 520 years and a U-Th age of 30,230 ± 160 years (*46*), consistent with the estimate of H3 calibrated age from ice core–marine correlation (*48*). This age is also supported by ^{14}C–U-Th datings of aragonite and organic material from Lake Lisan (*49*).

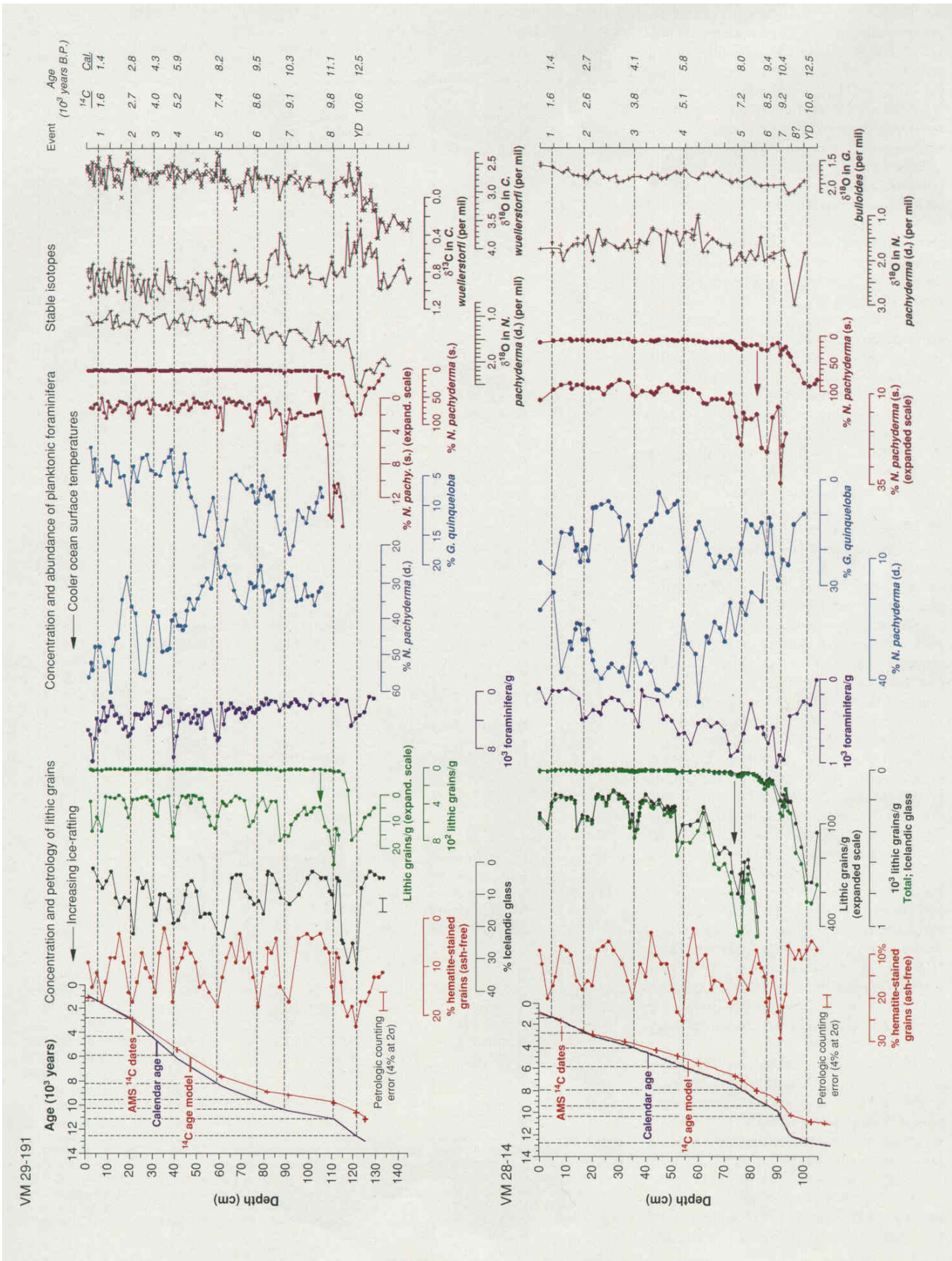

Fig. 2 (opposite page). Summary of proxy measurements in cores VM 29-191 and VM 28-14. Dashed lines are approximate peaks of the Holocene events, taking into account all of the records. In the lithic and *N. pachyderma* (s.) records, the Holocene events become evident only after expanding the horizontal scales. The record from VM 28-14 lacks the oldest event, most likely because of anomalously low sedimentation rates. Hematite-stained grain percentages are always given on an ash-free basis and are thus independent of variations in the material coming solely from Iceland. Petrologic counting error is from (*8*). Radiocarbon age– and calendar age–depth models are based on data in Table 1 and were produced by assuming linear sedimentation rates between dated intervals. After ~8200 years, $\delta^{13}C$ values in *C. wuellerstorfi* fall close to the modern value of ~1 per mil at the nearby GEOSECS site 23 (*45*).

Greenland and Svalbard (Fig. 1) and perhaps from farther north around the Arctic Ocean, where red beds also are present. The abrupt eastward and southward drops in tracer percentages almost certainly result from melting of ice along frontal systems where warm and cool surface waters mix (Figs. 1 and 4B). The low tracer percentages in Labrador Sea ice, therefore, likely reflect melting of tracer-rich ice in the Denmark Strait frontal system and the dearth of hematite-bearing sources of IRD around the Labrador Sea (*7*).

Hence, the North Atlantic's surface circulation must have alternated between two modes. At times of minimum concentrations of IRD and warmer sea surface temperatures at the coring sites, circulation probably was similar to today's, such that small amounts of tracer-poor ice from the Labrador Sea reached both coring sites. During the ice-rafting events, export of ice from the Labrador Sea may have increased, but surface waters of the Greenland-Iceland seas must have been advected much farther southward or southeastward than they are today, carrying tracer-rich ice to both coring sites (Fig. 1).

The changes in faunal assemblages during each ice-rafting event at VM 29-191 further support our circulation reconstruction and appear to restrict the IRD sources to surface waters in the southerly parts of the Greenland-Iceland seas near or within the frontal systems (Fig. 4A). Surface waters in the frontal systems tend to be quite productive (*19*), and their southward shifts, therefore, are consistent with prominent increases in foraminiferal concentrations associated with most of the IRD events at both sites (Fig. 2). The large magnitudes of the circulation changes are especially evident in the eastern North Atlantic where cool, ice-bearing surface waters shifted across more than 5° of latitude, each time penetrating well into what is at present the core of the warm North Atlantic Current.

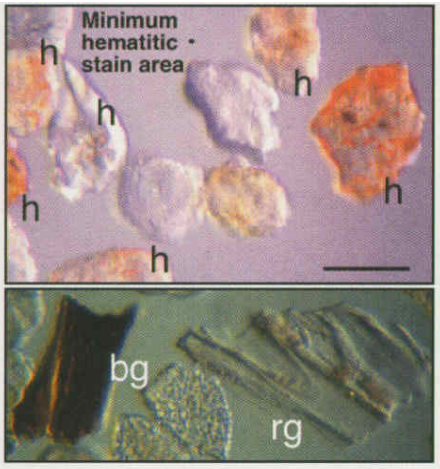

Fig. 3. Digitized photos of grains that compose the two tracers. Upper panel, hematite-stained grains (h); lower panel, Icelandic glass [clear rhyolitic (rg) and dark basaltic (bg) varieties]. Hematite-stained grains are defined as grains with at least one stained area the size of the small black dot, the minimum size at which hematite can be identified (the dot is set in the ocular of the microscope). Although the definition may seem at first to overdefine the grain type, 60 to 80% of non-Icelandic grains have no visible hematite staining. By counting all grains with identifiable hematite stain, therefore, we avoid rectifying the signal. Scale bar, 120 μm.

Fig. 4. (**A**) COADS temperature profile (*63*) as located in Fig. 1 and the latitudinal position of VM 29-191. This diagram provides an estimate of how much cooling might have occurred during each of the Holocene events at VM 29-191. The rationale is as follows: Within the Nordic Seas, there is only one place where the core top or "modern" abundances of *N. pachyderma* (s.), *G. quinqueloba*, and *N. pachyderma* (d.) are within the ranges of their values at the IRD peaks in VM 29-191. That is a rather narrow area just south of the Iceland-Faeroes Front, between ~60° and 62°N (*10*). On the basis of COADS temperature data averaged over the last 150 years, comparable to the duration of a single point in our records, the mean summer and winter temperature difference between the "modern analog" location and the location of VM 29-191 is between 1.5° and 2°C. If we assume, as the simplest alternative, that the temperature-faunal relation within the analog location can be transferred directly to the coring site, and that ambient temperatures at VM 29-191 were comparable to those of today, then probably 2°C of cooling at most occurred there during each Holocene event. (**B**) Cross section of the two petrologic tracers from section A–B (Fig. 1). All core top data from within the area of A–B were projected to the center along the green line. The cross sections demonstrate the difference in percentages of the two tracers north and south of the Iceland-Faeroes frontal system and the relation of those changes to the peak values of the tracers in our record from VM 29-191, as in Fig. 2.

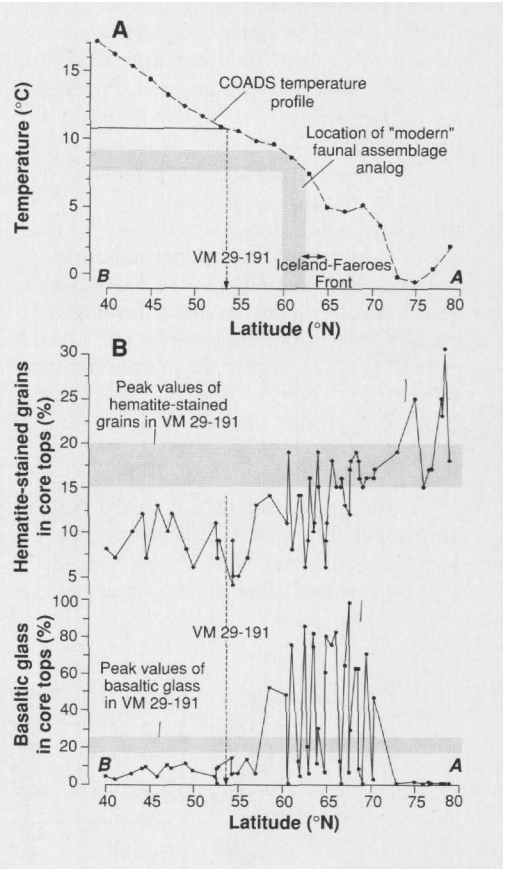

Thus, with a single mechanism—an oscillating ocean surface circulation—we can explain at once the synchronous ocean surface coolings, changes in IRD and foraminiferal concentrations, and changes in pet-

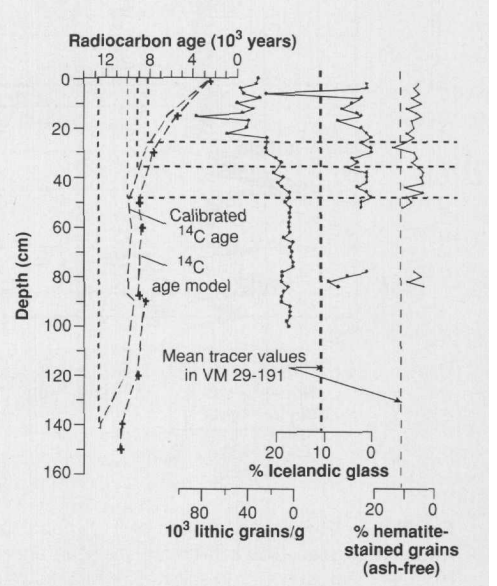

Fig. 5. Radiocarbon age– and calendar age–depth models for EW9303-GGC36 and our measurements of lithic grain concentrations and the two petrologic tracers (water depth, 3980 m). Mean values for the two tracers in VM 29-191 are from data in Fig. 2.

rologic tracers at both sites. Although we cannot rule out an increase in iceberg discharge from tidewater glaciers during the ice-rafting events, it is not required by the data in hand.

The deep southward advections of cooler and fresher surface waters into the core of the North Atlantic Current imply links with the North Atlantic's thermohaline circulation. For example, at VM 29-191, $\delta^{13}C$ values in the benthic foraminifera *Cibicidoides wuellerstorfi* decrease by ~0.5 to 0.6 per mil (Fig. 2), corroborating previous evidence that North Atlantic deep water (NADW) production was reduced during that climatic event (*20, 21*).

In the subsequent Holocene record, $\delta^{13}C$ values decrease by 0.4 to 0.5 per mil during event 7 at ~10,300 years (Fig. 2), suggesting reduced NADW production at that time as well. The absence of depletions in $\delta^{13}C$ values exceeding background noise (that is, depletions greater than ~0.3 per mil) during the other events does not necessarily rule out corresponding changes in NADW production; shifts in thermohaline circulation at those times may be recorded only in deeper, more sensitive sites near the present boundary between NADW and Southern Ocean water (*22*).

Correlations with the Greenland ice core. We also found evidence of a close link between the shifts in Holocene climate and atmospheric circulation above Greenland. In particular, the marine records exhibit a good correlation with the flux of non–sea salt K, one of the several constituents of atmospheric chemistry dissolved in Greenland ice and regarded as evidence of changes in loadings of terrigenous dust (*5*). With one exception, at 1400 years, the North Atlantic's Holocene events fall either on or close to peaks in that record (Fig. 6). The 1400-year event correlates with a prominent increase in the flux of another member of the geochemical series, sea salt Na, an indicator of storminess and entrainment of sea spray into the atmosphere (*5*). The Little Ice Age episode, which is clearly reflected in the geochemical series, is absent from our marine records because the core tops slightly predate that event.

O'Brien *et al.* (*5*) argued that the increases in soluble impurities in Holocene ice from Greenland probably occurred at times of lowered atmospheric temperatures. Their conclusion was based on evidence that certain of those shifts were associated with well-documented climatic deteriorations, such as the Little Ice Age, the 8200-year cooling event, and the Younger Dryas (*2, 23*). Our correlations with the ice core records, therefore, imply that during the

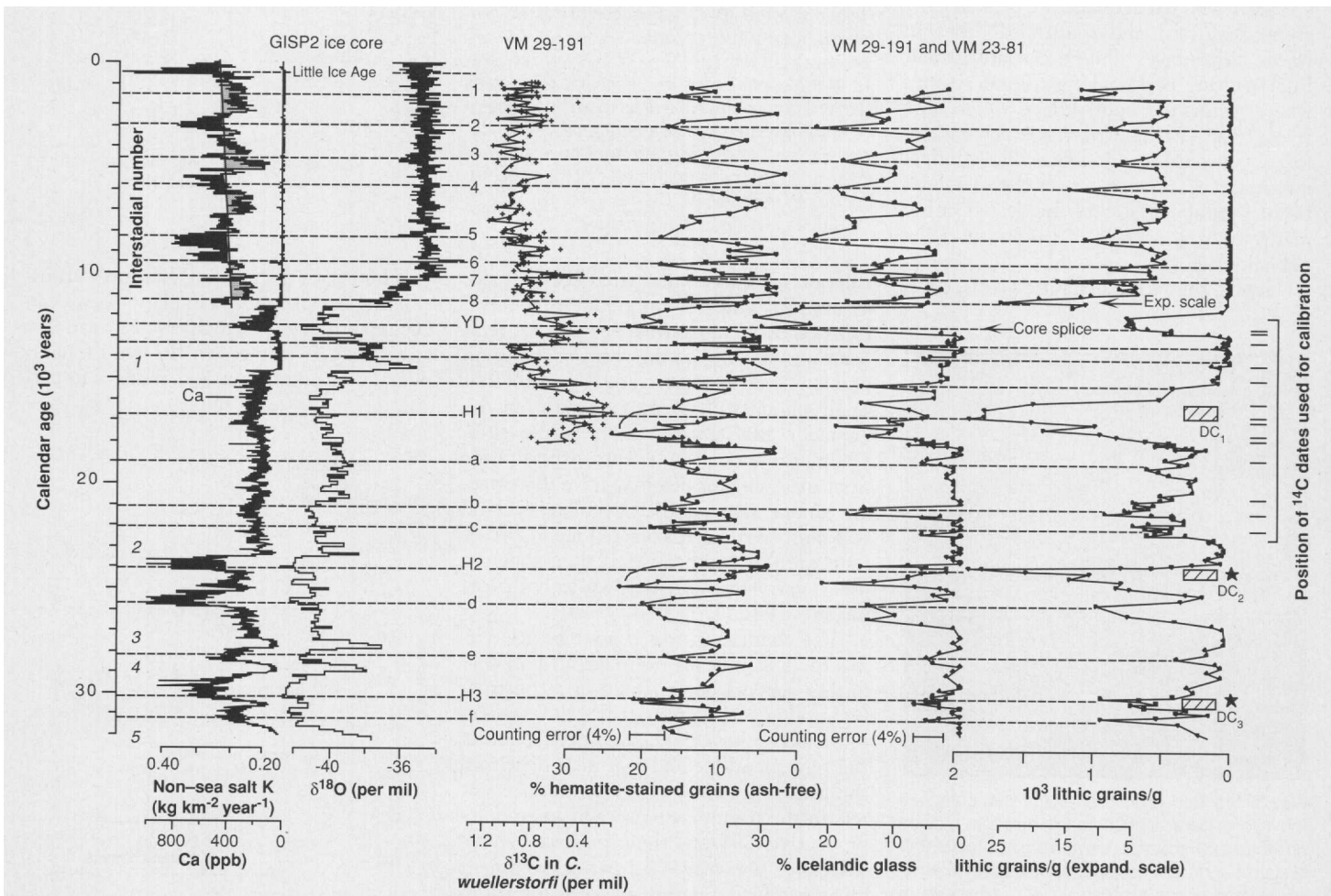

Fig. 6. Glacial-Holocene record of IRD, petrology, and $\delta^{13}C$ values in *C. wuellerstorfi*, placed on a calendar time scale and compared with GISP2 Ca, $\delta^{18}O$, and flux of non–sea salt K (*5, 47*). $\delta^{13}C$ values in *C. wuellerstorfi* are from VM 29-191; IRD and petrology are from the composite VM 29-191 and VM 23-81 record, spliced as indicated. The calendar time scale for the composite marine record was constructed as in (*24*); stars (at right) are ages for H2 and H3 used to extend the age model beyond the radiocarbon calibrations (see also Table 1). Calibration of the age of H3 is based on multiple criteria (*24*) and is ~4000 years younger than estimated by McIntyre and Molfino (*64*). Hatched boxes give positions of layers rich in detrital carbonate (DC). Interstadial numbers in ice core records are from (*65*). Holocene data are from VM 29-191; glacial data are from VM 23-81; the cores are joined at the core splice at the midpoint of the Younger Dryas event. Depletions in benthic $\delta^{13}C$ values associated with IRD events increase into the last glaciation, suggesting that the glacial amplification of the millennial-scale oscillator was linked to increasingly stronger decreases in NADW production.

Holocene, just as during the last glaciation, the North Atlantic's ocean surface and the atmosphere above Greenland were a coupled system undergoing recurring shifts on short, millennial scales.

A millennial-scale climate cycle. Despite a profound reorganization of climate at the onset of the Holocene, there is no statistical difference between pacings of the Holocene climate events and the rapid climate shifts that dominated the last glaciation. The evidence comes from a composite climate record we constructed by extending our measurements of IRD concentrations and petrologies back to ~32,000 years, the present limit of radiocarbon age calibrations. The glacial portion of the composite record is from VM 23-81 (Fig. 1) in which earlier work documented a series of fast-paced ice-rafting events (*7*). We increased the resolution of those events with additional measurements of lithic grain concentrations and their petrologies. The glacial records were placed on a calendar time scale, as described in Table 1 and (*24*), and joined to the Holocene record of VM 29-191, which is only a few kilometers away (Fig. 1) at the midpoint of the Younger Dryas detrital carbonate-lithic peak, dated at 10,880 radiocarbon years in both records (Fig. 6).

Thus, the composite record is based on the same proxies throughout. Moreover, all of the events reflect the same sense of climate change—that is, coolings (*25*). The three events between interstadials 1 and 2, equivalents of which have recently been identified in the Labrador Sea (*25*), demonstrate that the climate signal persists through the last glacial maximum where ice core $\delta^{18}O$, dissolved Ca (Fig. 6), and methane records (*26*) reveal no evidence of comparable climate variability. Why this is the case is unclear, but perhaps air masses carrying the signals were blocked from the interior of the ice cap by expansion of polar atmospheric circulation (*23*).

Using the procedure described in (*27*), we measured the pacing of the Holocene-glacial climate shifts in the most consistent and robust component of the composite record, the series of peaks in hematite-stained grains (Fig. 7A). For the glacial interval, the mean pacing is 1536 ± 563 years, essentially the same as a 1450-year cycle identified in the glacial portion of the Greenland Ice Sheet Project 2 (GISP2) geochemical series (*28*). For the Holocene interval, the mean pacing is 1374 ± 502 years. The standard deviations are from the means of the event pacings. Calendar age errors have been estimated back to 22,000 years, and for that interval, which makes up two-thirds of our total record, the errors are smaller than the standard deviations (compare Table 1 and Fig. 7A).

Thus, the pacings of the Holocene and glacial events are the same statistically, and together the two series constitute a cyclic signal centered on ~1470 ± 532 years. The signal persists across at least three major climate transitions: the Younger Dryas–Holocene transition, the deglaciation, and the boundary between marine isotope stages 2 and 3, which we have dated at ~30,000 years (Fig. 7A and Table 1). The implication of this finding is clear: The millennial-scale variability in our records reflects the presence of a pervasive, at least quasiperiodic, climate cycle occurring independently of the glacial-interglacial climate state.

Our composite record further suggests that the Holocene and glacial event pacings are nearly the same as those of the prominent Dansgaard/Oeschger $\delta^{18}O$ shifts of the last glaciation, especially in marine isotope stage 3 where they are best developed (Fig.

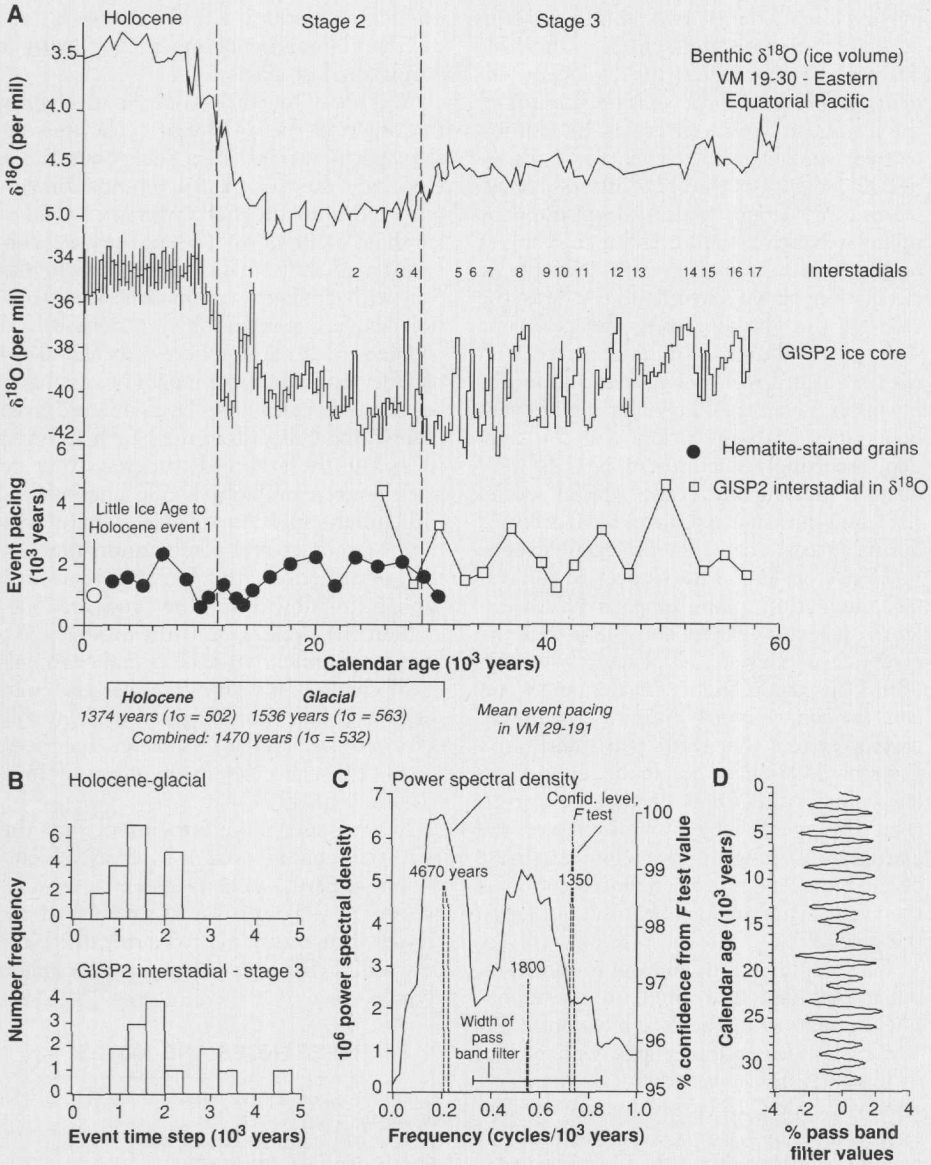

Fig. 7. (**A**) Time series of pacings of Holocene-glacial events from VM 29-191 and VM 23-81 (●), compared with pacings of numbered interstadials in GISP2 $\delta^{18}O$ (□) and benthic $\delta^{18}O$ in VM 19-30 (*66*). Pacings were calculated as in (*27*). The pacings of the Dansgaard/Oeschger cycles were obtained by measuring the time steps between numbered interstadials and placing the value at the midpoints between them. The time step to the Little Ice Age (○) is also shown for comparison with older event pacings. Mean values of event pacings are from the composite record of hematite-stained grains in Fig. 6. The calibrated time scale for VM 19-30 is from (*25*). On the basis of radiocarbon ages and their calibrations, the stage 2–stage 3 boundary is almost 6000 years older than given by SPECMAP tuning (*67*). (**B**) Histogram of Holocene-glacial IRD events and GISP2 interstadial events. (**C**) Multitaper spectral analysis (7 tapers) of time series of hematite-stained grains. (**D**) Filtered record of time series of hematite-stained grains.

7, A and B). That finding implies that Dansgaard/Oeschger cycles were not forced by internal instabilities of large ice sheets during glaciations, as some have suggested (3), but instead originated through processes linked to the climate cycle. Similarly, the consistent association of Heinrich events with cold phases of the cycle (Fig. 6) supports arguments by Bond and Lotti (7) that climate plays a fundamental role in their origin.

Finally, spectral analysis of the time series of hematite-stained grains by the multitaper method of Thompson (29) reveals that power is concentrated in two broad bands. One is centered at ~1800 years, near the mean of Holocene-glacial events, and the other is centered at ~4700 years (Fig. 7C). Cycles close to both have been noted previously in spectra from other paleoclimate records from the last glaciation (30). In addition, *F* variance ratio tests reveal lines with >95% probability at 4670, 1800, and 1350 years (Fig. 7C). Further corroboration of cyclicity close to the mean of the IRD events is given by applying a broad Gaussian bandpass filter to the record of hematite-stained grains centered on 1800 years (Fig. 7D).

Discussion. Our conclusion that millennial-scale shifts of Holocene and glacial climates originated fundamentally from the same forcing mechanism, a quasiperiodic climate cycle, has implications for the debate over the origin of abrupt climate changes and how those changes may influence future climates. The stability of the present climate in the North Atlantic must be considered in the context of millennial-scale variability in addition to interannual and interdecadal fluctuations, such as the North Atlantic Oscillation (31). For example, as originally suggested by Denton and Karlén (1), the Little Ice Age, a widespread climatic deterioration culminating about 300 years ago (32), was not an isolated event. Our records demonstrate that the time step separating the main phase of the Little Ice Age from the previous Holocene event (our event 1) is ~1100 years, falling well within the pacings of events in the composite record (Fig. 7A). The Little Ice Age, therefore, appears to have been the most recent cold phase in the series of millennial-scale cycles.

Whether the climatic amelioration since the Little Ice Age marks the onset of a warm phase of the cycle [for example, (33)] is, however, unclear. The series of climate events we have identified were not strictly periodic, and brief warmings often punctuated the cold phases of the millennial-scale fluctuations.

The 8200-year cooling, which is well documented by the only distinct Holocene $\delta^{18}O$ shift in Greenland ice, has received much attention because of its prominence in a growing number of other records (2). In our records, what is almost certainly the correlative of that cooling, event 5 (Fig. 6), is clearly part of the recurring series of climate shifts. We argue, therefore, that the origin of the 8200-year cooling is linked to the climate cycle and that its large amplitude in climate records reflects a mechanism that in some way amplified the climate signal at that time.

Finally, we are able to directly compare in the North Atlantic two prominent series of abrupt climate shifts from completely different climate states: the Holocene climate episodes and the marine imprint of the Dansgaard/Oeschger cycles. In addition to their similar pacings, events in both series document southward shifts of cooler, ice-bearing surface waters deep into the subpolar North Atlantic and a coupling of ocean surface circulation with atmospheric circulation above Greenland. As was the case for the glacial events, the Holocene shifts were abrupt, switching on and off within a century or two at least and probably faster, given the likely blurring of event boundaries by bioturbation (Fig. 2). Sudden, recurring reductions in NADW production accompanied the glacial cycles (34), and the same appears to have occurred during at least one of the Holocene events.

Hence, at least with respect to the surface circulation in the subpolar North Atlantic, it seems entirely consistent with the evidence to view the Holocene events as mini-Dansgaard/Oeschger cycles, and to regard the surface North Atlantic as a hydrographic system that shifts persistently in a Dansgaard/Oeschger-like mode, even when ice volumes are small. If that is correct, then the much larger amplitudes of the Dansgaard/Oeschger cycles relative to those of the Holocene reflect an amplification of the cyclic signal by a mechanism unique to the glaciation.

The amplifying mechanism is uncertain, but it may have been linked to thermohaline circulation in the North Atlantic. At VM 29-191, for example, large depletions of $\delta^{13}C$ values in *C. wuellerstorfi* during glaciation coincide with relatively large increases in IRD (Fig. 6). In cores from south of Iceland, similar shifts in $\delta^{13}C$ values in *C. wuellerstorfi* coincide with cold phases of Dansgaard/Oeschger cycles (34) and, by correlation, coincide with increases in IRD in VM 23-81 (Fig. 6) (7). During glaciation, the 1470-year cycle may have regulated iceberg discharges into the North Atlantic, thereby amplifying the signal through the impact of recurring increases in fresh water (icebergs) on rate of NADW production (35). An alternative mechanism is suggested by recent models demonstrating that a large-amplitude oscillatory mode can be induced in thermohaline circulation simply by increasing fresh water fluxes to the ocean, as would occur with growth of Northern Hemisphere ice sheets (36). The frequency of the oscillator could perhaps lock onto the frequency of a weak but persistent external forcing, such as the 1470-year cycle, in effect an amplification through entrainment or frequency locking. Regardless of the exact amplifying mechanism, the results of our study implicate ocean circulation as a major factor in forcing the climate signal and in amplifying it during the last glaciation.

We know too little thus far to identify the origin of the 1470-year cycle. Its constant pacing across major stage boundaries, especially the last glacial termination, almost certainly rules out any origin linked to ice sheet oscillations. Rather, the close correlation of shifts in ocean surface circulation with changes in atmospheric circulation above Greenland is consistent with a coupled ocean-atmosphere process. Coupled ocean-atmosphere modes of variability on decadal scales have been inferred from observational records in the North Atlantic (37), but those records are too short to assess longer, millennial-scale phenomena. Millennial-scale climate cycles may arise from harmonics and combination tones of the orbital periodicities, but cycles currently thought to fall within those bands are longer than the cycle we have identified (38). Forcing of millennial-scale climate variability by changes in solar output has also been suggested, but that mechanism is highly controversial, and no evidence has been found of a solar cycle in the range of 1400 to 1500 years (39).

In any case, if we are correct that the 1470-year climate cycle is a pervasive component of Earth's climate system, it must be present in previous glacial-interglacial intervals. If that turns out to be true, the cycle may well be the pacemaker of rapid climate change.

REFERENCES AND NOTES

1. G. H. Denton and W. Karlén, *Quat. Res.* **3**, 155 (1973).
2. R. B. Alley *et al.*, *Geology* **25**, 483 (1997).
3. W. S. Broecker, *Nature* **372**, 421 (1994).
4. T. Fronval and E. Jansen, *Paleoceanography* **12**, 443 (1997).
5. S. R. O'Brien *et al.*, *Science* **270**, 1962 (1995).
6. Core samples were collected with precision cutting tools to remove material in narrow slots at centimeter intervals. We avoided sampling the core's outer rind and obvious disturbances such as burrowing. All samples (dry) were weighed, then washed to separate the fine (<62 μm) from the coarse sediment fraction. All petrologic analyses were done in the 63- to 150-μm size range, which consistently contains at least a few hundred lithic grains. A portion of that grain fraction was placed on a glass slide (with glyc-

erin as a mounting medium) and 300 to 500 grains were counted per sample, using a line rather than point counting method. A key factor in our ability to measure certain tracers accurately is a specially prepared microscope. We placed a white reflector on the condenser lens and illuminated the sample slide from above with a halogen light source. By moving the substage reflector up and down, a position can be found that creates a strong impression of relief and brings into striking view details of surface textures and coatings on grains. The technique is especially useful for identifying hematite-stained grains, even when the stain is quite small (Fig. 3). Counting of lithic grain concentrations was done in the >150 μm fraction. To avoid errors introduced by splitting small grain populations, we did not split samples for this procedure. Counting of planktonic foraminiferal concentrations and abundances was done on splits of the >150 μm fraction. For the abundance measurements, 300 to 500 individuals were counted. Species in the >150 μm fraction were selected for planktonic and benthic isotopic measurements. All isotopic measurements were made at North Carolina State University by W.S. The samples were crushed and washed with reversed-osmosis water and air-dried at 65°C, and then 30- to 100-μg sample aliquots were isotopically analyzed in a Kiel Autocarbonate device attached to a FMAT 251 RMS. NBS-19, NBS-18, and the NCSU CM-1 marble standard were analyzed with every sample run for standard calibration and sample correction. During the period these samples were analyzed, for samples in the 10- to 100-μg size range the standard reproducibility was 0.07 per mil for ^{13}C and 0.08 per mil for ^{18}O. Planktonic isotopic analyses for VM 28-14 were made on 18 to 20 individuals per sample and were replicated at a number of depths. For VM 29-191, 10 replicate analyses were done on two or three individuals from each centimeter depth with the objective of investigating small-sample variability over time. Because those results showed no coherent relation to our other proxies, we combined all measurements from each centimeter with a mass balance equation using the sample size (micromolar) and the sample isotopic composition per mil, the results of which are shown in Fig. 2. The final result is equivalent to isotopically analyzing 20 planktonic individuals at once.

7. G. C. Bond and R. Lotti, *Science* **267**, 1005 (1995).
8. The counting error is the 2σ standard deviation for the mean of 20 replicate counts in each of two representative samples.
9. That we find any measurable record of drift ice as far south as 54°N is not as extraordinary as it might seem. Between about 1880 and the mid-1960s there were more than 20 iceberg sightings in the eastern North Atlantic between 45° and 60°N, and icebergs have been reported from as far south as Bermuda and the Azores (*40*). Even so, keeping in mind that the lithic grain concentrations are very low and that each sample integrates 50 to 100 years of time, the amounts of drifting ice reaching either site, even at peak concentrations, must have been small, and certainly much less than during the glaciation.
10. T. Johannessen, E. Jansen, A. Flatoy, A. C. Raveo, in *Carbon Cycling in the Glacial Ocean: Constraints on the Ocean's Role in Global Change*, R. Zahn *et al.*, Eds. (NATO ASI Series, Vol. I 17, Springer-Verlag, Berlin, 1994), pp. 61–85.
11. S. R. Epstein, R. Buchsbaum, H. A. Lowenstam, H. C. Urey, *Geol. Soc. Am. Bull.* **64**, 1315 (1953).
12. M. Sarnthein *et al.*, *Paleoceanography* **10**, 1063 (1995); G. Wu and C. Hillaire-Marcel, *Geochim. Cosmochim. Acta* **58**, 1303 (1994).
13. D. W. Oppo, M. Horowitz, S. J. Lehman, *Paleoceanography* **12**, 51 (1997).
14. T. B. Kellogg, in *Climatic Changes on a Yearly to Millennial Basis*, N.-A. Mörner and W. Karlén, Eds. (Reidel, Dordrecht, Netherlands, 1984), pp. 123–133.
15. L. Labeyrie *et al.*, *Philos. Trans. R. Soc. London* **348**, 255 (1995).
16. B. E. Viekman and K. D. Baumer, *International Ice Patrol Technical Report 95-03* (Department of Transportation, U.S. Coast Guard, International Ice Patrol, 1995).
17. Most of the cores (indicated by solid dots in Fig. 1) have Holocene sections, documented on the basis of radiocarbon dating, isotopic measurements, or the presence of ash layer 1 (~10,000 years) at depths of tens of centimeters. The existence of Holocene sections in the remainder, indicated by plus signs, is inferred from distinct color patterns and bulk carbonate measurements (*41*). Core top ages likely vary from close to the present to perhaps a few thousand years; on average, then, the core top petrologic data reflect distributions of the tracers over time as well as over a large geographic area. The petrographic analyses of each core top lithic sample were done in the same way as for VM 29-191 and VM 28-14.
18. There probably were no tidewater glaciers in Iceland, at least during the middle and late parts of the Holocene, ruling out transport of debris to the sites by Icelandic icebergs; direct transport in eruption clouds is also ruled out by the large size of clasts (coarsest grains typically are 0.5 to 1 mm) and by evidence that only two of the six largest Holocene eruptions in Iceland are correlative with the petrologic events (*42*). The only plausible mechanism, therefore, is eruption of Icelandic volcanic material onto nearby sea ice (and probably glacier ice as well) and subsequent transport of that ice in surface currents to the coring sites. Explosive eruptions from volcanoes such as Hekla, Katla, and Grimsvotn occur once every 20 to 30 years or so in Iceland (*43*), and the Icelandic lithic grains at both sites are dominantly (70 to 95%) clear rhyolitic glass shards, the characteristic product of explosive eruptions in silicic volcanoes. The importance of our interpretation of the Icelandic IRD is that its increases at VM 28-14 require increases in drift ice within reach of eruption clouds to the east. Hence, changes in surface hydrography favoring preservation and transportation of drift ice in the western North Atlantic must have taken place, at the very least, from Denmark Strait to the vicinity of Iceland or Jan Mayen.
19. S. Sathyendranath, A. Longhurst, C. M. Caverhill, T. Platt, *Deep Sea Res. Pt. 1*, **42**, 1773 (1995).
20. The carbon isotopic composition of *C. wuellerstorfi* appears to record the ^{13}C of total CO_2 of sea water, and therefore is taken as a proxy of the nutrient content of that water (*44*). Today, VM 29-191 lies within NADW, which is nutrient-depleted and hence $\delta^{13}C$-enriched; below the depth of the core are modified waters of Southern Ocean origin, which are nutrient-enriched and $\delta^{13}C$-depleted (*45*). Variations in the $\delta^{13}C$ of that foraminifera are related to shifts in the rate of production of NADW and hence in the rate of convective overturning and thermohaline circulation in the North Atlantic (*34, 44*).
21. E. Boyle, *Philos. Trans. R. Soc. London* **348**, 243 (1995).
22. M. S. McCartney, *Prog. Oceanogr.* **29**, 283 (1992).
23. P. A. Mayewski *et al.*, *Science* **263**, 1747 (1994).
24. The calendar age model in the composite record for the interval between the Younger Dryas and 18,000 radiocarbon years was constructed by linear interpolation between radiocarbon dates from VM 23-81 calibrated following Bard *et al.* (*46*) (Table 1). For the remainder of the record, we transferred the GISP2 ages of Heinrich events 2 and 3 (H2 and H3) (*47*) into their equivalent levels in VM 23-81 (Table 1) (*48*) and interpolated linearly between the two ages. Our estimate of the age of H3 is corroborated by calibrated radiocarbon measurements in Barbados corals (Table 1) and by paired U-Th–^{14}C measurements in aragonite from Lake Lisan in the Dead Sea Rift (*49*). Detrital carbonate at the Younger Dryas level was deposited rapidly and is widespread, extending from the eastern North Atlantic to sources in Hudson Strait and Cumberland Strait (*50*); it serves as an excellent chronostratigraphic marker. Calibrations of radiocarbon ages in VM 19-30 (Table 1) at 100 and 150 cm are from (*46*). Remaining calibrations are from the age model for the Holocene-glacial composite record as described above.
25. The Heinrich events are tied to well-documented lowerings of atmospheric and ocean surface temperatures and to large reductions in the rate of NADW formation (Fig. 6) (*34*). The two distinct ice-rafting peaks between interstadial 1 and the Younger Dryas, dated at ~13,200 and ~14,000 calendar years (~11,300 and 12,000 ^{14}C years), are accompanied by increases in *N. pachyderma* (s.) measured in the same core (*51*), and they are coincident with prominent decreases in $\delta^{18}O$ in Greenland ice (Fig. 6). Evidence of coolings at about the same times have been found in other deep sea cores from the North Atlantic (*52*) and the Nordic Seas (*53*) and in pollen and glacial records in Europe and North America (*53*). From 23,000 calendar years to the end of the record, the IRD-petrologic episodes between Heinrich events also occur at times of maxima in abundances of *N. pachyderma* (s.) (*7*) and at times of prominent cold phases in the ice core $\delta^{18}O$ records (Fig. 6). We also find distinct IRD events punctuating prolonged stadials, such as between interstadials 2 and 3 and interstadials 4 and 5. There, the IRD-petrologic peaks correspond to prominent increases in dissolved Ca (Fig. 6) and in the polar circulation index (*23*), suggesting a close association of the marine events with expansion of polar circulation above the ice cap. Within the long interval between interstadials 1 and 2, we have identified four other IRD-petrologic events in addition to H1. The *N. pachyderma* (s.) abundances are saturated through the entire interval, preventing reliable estimates of changes in sea surface temperatures. The youngest of the four events, dated at ~15,200 calendar years (~12,900 ^{14}C years), however, is correlative with glacial advances in the U.S. midwest [for example, Port Huron Stade (*54*)], with a glacial readvance on the Scotian shelf (*55*), and with a Heinrich-like cooling and ice-rafting event identified on the Scotian Slope (*56*). The other three events, a, b, and c, previously identified by Bond and Lotti (*7*) and dated at about 19,000, 21,000, and 22,000 calendar years (~16,500, 17,500, and ~18,600 ^{14}C years), are present in IRD records from a number of other sites in the subpolar North Atlantic and GIN Seas (*57*), and they also appear in magnetic susceptibility records from the Labrador Sea (*58*). Two of these widespread events, a and c, are correlative with prominent coolings identified in pollen records from a long lacustrine sequence in northern Norway (*59*). There is evidence that the two older events, b and c, may even be correlative with glacial advances in the Southern Hemisphere, implying a bihemispheric symmetry of the abrupt changes (*60*).
26. E. J. Brook, T. Sowers, J. Orchardo, *Science* **273**, 1087 (1996).
27. We define event pacing as the time separating adjacent peaks placed at the midpoints between the peaks (Fig. 6). We define peaks as maxima with at least two points and amplitudes equal to or exceeding the 2σ counting error [4% (*8*)]; the measure of separation is made between maxima in peak percentage. At the levels of H1 and H2, the sharp decreases in percentages of the two petrologic tracers reflect dilution by massive amounts of IRD discharged from the Labrador Sea (*7*), and we place the peaks for those two events at maxima in the lithic grain concentrations (Fig. 6).
28. P. A. Mayewski *et al.*, *J. Geophys. Res.*, in press.
29. D. J. Thompson, *Proc. IEEE* **70**, 1055 (1982).
30. P. Yiou and J. Jouzel, *Geophys. Res. Lett.* **22**, 2179 (1995); L. D. Keigwin and G. A. Jones, *J. Geophys. Res.* **99**, 12397 (1994); E. Cortijo, P. Yiou, L. Labeyrie, M. Cremer, *Paleoceanography* **10**, 911 (1995).
31. J. C. Rogers, *J. Clim.* **3**, 1364 (1990).
32. J. M. Grove, *The Little Ice Age* (Methuen, London, 1988).
33. L. D. Keigwin, *Science* **274**, 1504 (1996).
34. D. W. Oppo and S. J. Lehman, *Paleoceanography* **10**, 901 (1995).
35. S. Rahmstorf, *Nature* **378**, 145 (1995); S. Manabe and R. J. Stouffer, *Paleoceanography* **12**, 321 (1997); T. F. Stocker, D. G. Wright, W. S. Broecker, *ibid.* **7**, 529 (1992).
36. K. Sakai and W. R. Peltier, *J. Clim.* **10**, 949 (1997); E. Tziperman, *Nature* **386**, 592 (1997); A. J. Weaver and T. M. C. Hughes, *ibid.* **367**, 447 (1994).
37. R. T. Sutton and M. R. Allen, *Nature* **388**, 563 (1997); Y. Kushnir, *J. Clim.* **7**, 141 (1994).
38. P. Pestiaux, I. Van der Mersch, A. Berger, J. C.

Duplessy, *Clim. Change* **12**, 9 (1988); P. Yiou *et al.*, *J. Geophys. Res.* **96**, 20365 (1991).
39. M. Stuiver and T. F. Braziunas, *The Holocene* **3**, 289 (1993); E. A. Frieman, *Solar Influences on Global Change* (National Academy Press, Washington, DC, 1994).
40. *Oceanographic Atlas of the North Atlantic* (U.S. Naval Oceanographic Office, Washington, DC, 1968); J. E. Murry, in *Ice Seminar*, V. E. Bohme, Ed. (Canadian Institute of Mining and Metallurgy, Washington, DC, 1969), pp. 3–18.
41. T. B. Kellogg, thesis, Columbia University (1973).
42. A. J. Dugmore, G. Larsen, A. J. Newton, *The Holocene* **5**, 257 (1995); S. Thorarinsson, in *Tephra Studies*, S. Self and R. S. J. Sparks, Eds. (Reidel, Dordrecht, Netherlands, 1981), pp. 109–134; R. A. J. Cas and J. V. Wright, *Volcanic Successions* (Allen and Unwin, Winchester, MA, 1987); H. J. Gudmundsson, *Quat. Sci. Rev.* **16**, 81 (1997).
43. T. Simkin *et al.*, *Smithsonian Institution Volcanoes of the World* (Hutchinson Ross, Stroudsburg, PA, 1981).
44. E. A. Boyle and L. D. Keigwin, *Nature* **330**, 35 (1987).
45. P. Kroopnick, *Earth Planet. Sci. Lett.* **49**, 469 (1980).
46. E. Bard, M. Arnold, R. G. Fairbanks, B. Hamelin, *Radiocarbon* **35**, 191 (1993); M. Stuiver and J. Reimer, *ibid.*, p. 215.
47. M. J. Bender *et al.*, *Nature* **372**, 663 (1994).
48. G. C. Bond *et al.*, *ibid.* **365**, 143 (1993).
49. S. Goldstein, personal communication.
50. J. T. Andrews *et al.*, *Paleoceanography* **10**, 943 (1995).
51. S. J. Lehman and L. D. Keigwin, *Nature* **356**, 757 (1992).
52. H. P. Sejrup, H. Haflidason, D. K. Kristensen, *J. Quat. Sci.* **10**, 385 (1995).
53. N. Koç, E. Jansen, M. Hald, L. Labeyrie, in *Late Quaternary Palaeoceanography of the North Atlantic Margins*, J. T. Andrews, W. E. N. Austin, H. Bergsten, A. E. Jennings, Eds. (Geological Society Special Publication 111, 1996), pp. 177–185.
54. G. H. Denton and T. J. Hughes, in *The Last Great Ice Sheets* (Wiley, New York, 1981).
55. R. R. Stea, R. Boyd, O. Costello, G. B. J. Fader, D. B. Scott, in (*53*), pp. 77–101.
56. L. D. Keigwin and G. A. Jones, *Paleoceanography* **10**, 973 (1995).
57. R. Stein, S.-I. Nam, H. Grobe, H. Hubberten, in (*53*), pp. 135–151; T. Fronval and E. Jansen, *Nature* **383**, 806 (1996); H. Haflidason, H. P. Sejrup, D. K. Kristensen, S. Johnsen, *Geology* **23**, 1059 (1995).
58. J. S. Stoner, J. E. T. Channell, C. Hillaire-Marcel, *Paleoceanography* **11**, 309 (1996).
59. T. Alm, *Boreas* **22**, 171 (1993).
60. T. V. Lowell *et al.*, *Science* **269**, 1541 (1995).
61. I. M. Lagerklint, thesis, University of Maine (1995).
62. E. Bard *et al.*, *Earth Planet. Sci. Lett.* **126**, 275 (1994).
63. S. D. Woodruff, R. J. Slutz, R. L. Jenne, P. M. Steurer, *Bull. Am. Meteorol. Soc.* **68**, 521 (1987).
64. A. McIntyre and B. Molfino, *Science* **274**, 1867 (1996).
65. W. Dansgaard *et al.*, *Nature* **364**, 218 (1993).
66. N. J. Shackleton, J. Imbrie, M. A. Hall, *Earth Planet. Sci. Lett.* **65**, 233 (1983).
67. D. G. Martinson *et al.*, *Quat. Res.* **27**, 1 (1987).
68. We thank G. Kukla, J. Lynch-Stieglitz, and A. Van Geen for comments on the manuscript. Supported in part by grants from NSF and the National Oceanic and Atmospheric Administration. Support for the core curation facilities of the Lamont-Doherty Earth Observatory Deep-Sea Sample Repository is provided by NSF through grant OCE94-02150 and the Office of Naval Research through grant N00014-96-I-0186. This is L-DEO contribution 5714.

29 July 1997; accepted 26 September 1997